Three-Dimensional Solution Structure of *Callinectes sapidus* Metallothionein-1 Determined by Homonuclear and Heteronuclear Magnetic Resonance Spectroscopy[†,‡]

Surinder S. Narula,[▽,§] Marius Brouwer,[∥] Yuxin Hua,[▽] and Ian M. Armitage*[,▽,⊥]

Departments of Pharmacology and Diagnostic Radiology, Yale University School of Medicine, 333 Cedar Street, P.O. Box 208066, New Haven, Connecticut 06520-8066, and Duke University Marine Laboratory, Beaufort, North Carolina 28516

Received July 13, 1994; Revised Manuscript Received October 6, 1994[⊗]

ABSTRACT: Metallothionein is a cysteine-rich metal-binding protein whose biosynthesis is closely regulated by the level of exposure of an organism to zinc, copper, cadmium, and other metal salts. The metallothionein from *Callinectes sapidus* is known to bind six divalent metal ions in two separate metal-binding clusters. Heteronuclear $^{1}H-^{113}Cd$ and homonuclear $^{1}H-^{1}H$ NMR correlation experiments have been used to establish that the two clusters reside in two distinct protein domains. The three-dimensional solution structure of the metallothionein has been determined using the distance and angle constraints derived from these two-dimensional NMR data sets and a distance geometry/simulated annealing protocol. There are no interdomain short distance (≤4.5 Å) constraints observed in this protein, enabling the calculation of structures for the N-terminal, β domain and the C-terminal, α domain separately. A total of 18 structures were obtained for each domain. The structures are based on a total of 364 experimental NMR restraints consisting of 277 approximate interproton distance restraints, 12 χ^1 and 51 ϕ angular restraints, and 24 metal-to-cysteine connectivities obtained from $^{1}H-^{113}Cd$ correlation experiments. The only element of regular secondary structure in either of the two domains is a short segment of helix in the C-terminal α domain between Lys42 and Thr48. The folding of the polypeptide backbone chain in each domain, however, gives rise to several type I β turns. There are no type II β turns.

Metal ions are both essential and toxic elements. They are integral, functional components of many enzymes and transcriptional regulatory proteins (Coleman, 1992; O'Halloran, 1993). On the other hand, the binding of metals to biological macromolecules often perturbs their function (Vallee & Ulmer, 1972), and metal-catalyzed formation of oxygen-derived free radicals has been implicated in a wide variety of pathological conditions as well as in mutagenicity and carcinogenicity (Halliwell & Gutteridge, 1990). To cope with potentially hazardous levels of heavy metal ions, organisms appear to have developed an integrated, metal-regulatory network to control the concentration and availability of these elements. A major component of this network is a family of low molecular weight, cysteine-rich, metal-binding proteins called metallothioneins (MTs)[1] (Kägi & Kojima, 1987). These proteins are expressed in many different cell lines and tissues following exposure to heavy metals, glucocorticoid hormones, interferon, interleukin-I, bacterial endotoxin, UV radiation, and oxidative stress (Hamer, 1986; Cousins, 1985; Engel & Brouwer, 1989; Bauman et al., 1991). The expression of MT genes is regulated at the transcriptional level, through interactions between cis-acting metal- and glucocorticoid-responsive elements and trans-acting, DNA-binding, metal-regulatory (metallo)proteins (Thiele, 1992; Seguin, 1991; Butler & Thiele, 1991; Andersen et al., 1990). In mammals, there are at least two major isoforms of MT. Induction of these isoforms can be metal and hormone specific (Richards et al., 1984). Differential induction of MT isoforms by Cu and Cd has been observed in human cell lines and in blue crab (*Callinectes sapidus*) tissues (Sadhu & Gedamu, 1988; Brouwer et al., 1992). These observations suggest that different MT isoforms perform distinct functions in metal homeostasis and detoxification.

NMR spectroscopy (Otvos & Armitage, 1980; Messerle et al., 1990) and X-ray diffraction studies (Robbins et al.,

[†] This work was supported by grants from the National Institutes of Health to I.M.A. (DK18778) and to M.B. (ESO4074). NMR instrumentation and computational facilities were provided by NIH (RR03475), NSF (DMB8610557), and ACS (RD259).

[‡] Crystallographic coordinates have been submitted to the Brookhaven Protein Data Bank under the following accession numbers. CD-6 metallothionein-1 (MT-1), α domain: minimized average coordinates, T5654 1DMC; 18 model coordinates, T5655 1DMD; restraints, T5656 1DMD-MR. MT-1, β domain: minimized average coordinates, T5657 1DME; 18 model coordinates, T5658 1DMF; restraints, T5659 1DMF-MR.

* To whom correspondence should be addressed at Department of Pharmacology.

[▽] Department of Pharmacology, Yale University School of Medicine.

[§] Ariad Pharmaceuticals, 26 Landsdowne Street, Cambridge, MA 02139.

[∥] Duke University Marine Laboratory.

[⊥] Department of Diagnostic Radiology, Yale University School of Medicine.

[⊗] Abstract published in *Advance ACS Abstracts,* November 15, 1994.

[1] Abbreviations: Cd-MT, cadmium(II) substituted blue crab metallothionein; COSY, homonuclear two-dimensional correlated spectroscopy; DQF-COSY, double-quantum filtered COSY; HMQC, heteronuclear multiple quantum coherence spectroscopy; MT, metallothionein; NMR, nuclear magnetic resonance; NOE, nuclear Overhauser effect; NOESY, two-dimensional NOE spectroscopy; ppm, parts per million; PE-COSY, primitive-exclusive two-dimensional correlated spectroscopy; relay-COSY, two-dimensional relayed *J*-correlated spectroscopy; TOCSY (HOHAHA), two-dimensional total correlation spectroscopy (homonuclear Hartmann−Hahn); TPPI, time-proportional phase incrementation; WT, wild type.

0006-2960/95/0434-620$09.00/0

1991) have shown that Cd_5Zn_2-MT of various mammalian species is a dumbbell-shaped molecule, composed of an N-terminal 9-cysteine/3-metal cluster and a C-terminal 11-cysteine/4-metal cluster. No interdomain interactions were reported in these studies. The cadmium thiolate clusters, especially the three-metal cluster in mammalian MT, possess a high degree of dynamic freedom. The continual breaking and re-forming of coordination bonds allows for facile intramolecular metal exchange within the N-terminal cluster and intermolecular metal exchange between clusters of different MT molecules (Vasak, 1986; Otvos et al., 1989). This strongly suggests that the two domains of mammalian MTs have evolved to perform different functional roles. The kinetically labile N-terminal domain may function in metal-exchange processes, whereas the kinetically more stable C-terminal domain may be important in detoxification. Studies on mutant MTs in which cysteine residues in either domain have been replaced corroborate this hypothesis (Cismowski & Huang, 1991; Cismowski et al., 1991). Whether intracellular metal exchange occurs between MTs or between MT and other (apo)metalloproteins is unknown. However, recent studies with mammalian cell lines and marine crustacea suggest that copper exchange takes place between Cu(I)-MT and the tripeptide glutathione (Freedman et al., 1989; Brouwer & Brouwer-Hoexum, 1991; Brouwer et al., 1993).

Earlier studies in marine crustacea identified two Cd-inducible MT isoforms in the mud crab, *Scylla serrata* (Lerch et al., 1982), and the blue crab, *Callinectes sapidus* (Brouwer et al., 1984). ^{113}Cd NMR had been used to determine the structure of the multiple Cd(II) binding sites in the two isoproteins of the mud crab (Otvos et al., 1982). The application of homonuclear ^{113}Cd decoupling techniques showed that the mud crab MT-1 and MT-2 contained two distinct three-metal clusters. It is significant that, despite the evolutionary distance between the mud crab and the higher vertebrates, the metals in MTs from both invertebrates and vertebrates are arranged in two distinct metal−thiolate clusters with the structures of both clusters in crab MT being apparently similar to the three-metal cluster in the mammalian N-terminal domain. Whether the two metal clusters of mud crab MT were located in two different protein domains, and whether the metal exchange rates in the two clusters were different, as in the mammalian MTs, was unknown. In fact, to date, there have been no high-resolution structural studies (X-ray or NMR) reporting on the three-dimensional structure of any invertebrate MT.

In this paper, we report on the three-dimensional solution structures of blue crab MT-1 determined using two-dimensional $^1H-^1H$ homonuclear and $^1H-^{113}Cd$ heteronuclear NMR spectroscopy and a distance geometry/simulated annealing structure calculation approach.

MATERIALS AND METHODS

Sample Preparation. CdMT-1 from blue crab was purified using standard procedures (Brouwer et al., 1986; 1992). Four separate preparations of the samples were pooled and concentrated with an Amicon apparatus and a YM-1 membrane under argon pressure. The final protein concentration was 4 mM in 20 mM KP_i at pH 7.0. The experimental procedure for preparing the enriched $^{113}CdMT$-1 sample was as described earlier (Narula et al., 1993).

NMR Methods. ^1H NMR spectra were recorded on a Bruker AM500 NMR spectrometer. All the measurements were made using 0.5 mL of the protein sample contained in a 5-mm NMR tube. To resolve the ^1H spectral overlap, data were acquired at temperatures of 5, 10, and 30 °C in H_2O (i.e., 90% H_2O and 10% ^2H_2O) and 99.8% ^2H_2O. All of the two-dimensional (2D) spectra were acquired in the phase-sensitive mode using TPPI (Marion & Wüthrich, 1983). The water resonance was suppressed in all the experiments by its irradiation during a relaxation delay of 0.9−1.5 s. In $^1H-^1H$ 2D NMR experiments, a spectral width of 6024 Hz was covered in both dimensions with the carrier set on the water resonance. The decoupler was also set on the water resonance, and both transmitter and decoupler channels were phase locked to obtain a better suppression of the water resonance (Zuiderweg et al., 1986).

For COSY (Aue et al., 1976; Bax & Freeman, 1981), DQF-COSY (Piantini et al., 1982; Rance et al., 1983), relay-COSY (Eich et al., 1982; Bax & Drobny, 1985), and PE-COSY (Mueller, 1987; Marion & Bax, 1988), 440−576 increments in t_1 (32−128 scans per increment) and 2048 complex data points in t_2 were acquired. For NOESY (Jeener et al., 1979; Kumar et al., 1980), mixing times between 60 and 200 ms were used, and for TOCSY (Bax & Davis, 1985), MLEV-17 spin-lock times between 55 and 155 ms were used with 400−540 increments in t_1 (64−228 scans per increment) and 2048 complex data points in t_2. To eliminate base-line distortions for all NOESY and TOCSY spectra, the acquisition parameters, in particular the relative receiver phase and the delay between the last pulse and the start of the acquisition, were adjusted such that the zero- and first-order phase corrections along ω_2 were 90° and 180°, respectively (Marion & Bax, 1988). The data were processed with the Felix program (Biosym Technologies, San Diego, CA) running on a Sun Sparc 1+ computer. For COSY and DQF-COSY data sets, the time domain signal along ω_2 was multiplied by a sine bell of 0° before Fourier transformation for resolution enhancement. The signal along ω_1 was similarly multiplied by a sine bell of 0° and then zero filled to 2048 complex points, resulting in a 2K × 2K real matrix. For relay-COSY data sets, the time domain signals along ω_2 and ω_1 were multiplied by a sine bell of 0° and a shifted sine bell of 3°, respectively, before Fourier transformation for resolution enhancement. For the PE-COSY data set, the time domain signals along both ω_2 and ω_1 were multiplied by a shifted sine bell of 45° before Fourier transformation for resolution enhancement. For NOESY and TOCSY, the time domain signal along ω_2 was multiplied by a sine bell or a shifted sine bell of 22° before Fourier transformation for resolution enhancement. The signal along ω_1 was similarly multiplied by a sine bell or a shifted sine bell of 22° and then zero filled to 2048 complex points, resulting in a 2K × 2K real matrix.

For ^1H NMR chemical shift referencing, the residual water resonance was assigned to 4.75 ppm in a 30 °C spectrum for samples in 99.8% ^2H_2O to compensate for isotope effects. The most upfield resonance at 0.97 ppm, which is assigned to the γ-CH_3 of V10, was calibrated with respect to the HDO resonance at 30 °C and thereafter used as the reference at other temperatures (Table 1). The COSY spectrum is shown as contour plots with both positive and negative levels. The horizontal and vertical axes represent ω_2 and ω_1, respectively. The experimental details for the $^1H-^{113}Cd$ HMQC experiments carried out on ^{113}Cd-enriched metallothionein were as reported in an earlier publication (Narula et al., 1994).

Table 1: ^{1}H Chemical Shifts (in ppm) for Cadmium-Substituted Blue Crab Metallothionein-1, pH 7.0, 30 °C, in 20 mM Potassium Phosphate (Backbone Protons Are Also Listed at 10 °C)

	NH		H^α			
residue	10 °C	30 °C	10 °C	30 °C	H^β	others[a]
P1			4.50	4.50	2.15, 2.48	H^γ 2.12; H^δ 3.47
G2	8.02	8.00	4.18	4.19		
P3			4.53	4.53	2.31	H^γ 1.96, 2.09; H^δ 3.55, 3.87
C4	7.48	7.54	5.02	4.97	3.05(*R*), 3.17(*S*)	
C5	8.74	8.55	4.66	4.68	3.63	
N6[c]	8.26	8.26	4.46	4.45	2.64, 2.70	$N^\delta H$ 6.92, 7.47
D7	8.68	*b*	4.65	*b*	2.67, 2.72	
K8	7.67	7.67	4.33	4.33	1.75, 1.88	H^γ 1.12, 1.26; H^δ 1.62; H^ϵ 2.93
C9	8.89	9.04	4.53	4.57	2.95, 3.83	
V10	7.89	7.85	4.77	4.76	2.67	$C^\gamma H_3$ 0.97, 1.08
C11	8.36	8.37	4.64	4.63	2.65(*S*), 2.82(*R*)	
Q12[d]	8.85	8.75	4.15	4.19	2.11, 2.21	H^γ 2.48
E13	7.78	7.65	4.44	4.46	2.07, 2.20	H^γ 2.34
G14	7.94	7.97	4.15	4.13		
G15	8.21	8.12	3.69, 4.34	3.68, 4.35		
C16	8.74	8.54	4.87	4.90	3.18(*S*), 3.26(*R*)	
K17	9.59	9.45	4.68	4.67	1.57	H^γ 1.49; H^δ 1.69; H^ϵ 3.06
A18	8.76	8.54	4.16	4.17	1.41	
G19	8.98	8.82	3.76, 4.13	3.73, 4.15		
C20	7.23	7.22	3.95	3.96	2.91(*R*), 3.11(*S*)	
Q21	9.79	9.57	4.45	4.49	1.75	H^γ 2.44, 2.66; $N^\epsilon H$ 6.87, 7.77
C22	9.46	9.38	4.35	4.36	2.78(*S*), 3.24(*R*)	
T23	8.90	8.72	4.47	4.47	4.66	$C^\gamma H_3$ 1.35
S24	9.34	9.35	4.56	4.58	3.90, 4.04	
C25	*b*	7.46	5.02	5.03	3.01(*R*), 3.66(*S*)	
R26[c]	8.26	8.25	4.46	4.48	1.64	H^γ 1.11, 1.49; H^δ 3.20
C27	9.26	9.02	3.74	3.81	2.94(*R*), 3.24(*S*)	
S28	8.04	7.92	4.57	4.59	3.88, 3.94	
P29		4.33		4.33	1.77, 2.17	H^γ 2.41; H^δ 3.66, 3.85
C30	9.79	*b*	4.71	4.71	3.27(*R*), 3.59(*S*)	
Q31[d]	8.88	8.75	4.21	4.19	2.22	H^γ 2.52; $N^\epsilon H$ 7.03, 7.73
K32	9.40	9.35	4.29	4.31	1.92	H^δ 1.69; H^ϵ 3.11
C33	7.98	7.93	4.40	4.42	2.86(*S*), 3.71(*R*)	
T34	7.90	7.85	3.85	3.86	4.19	$C^\gamma H_3$ 1.27
S35	8.29	*b*	4.63	4.66	4.02	
G36	7.40	7.36	3.50, 4.36	3.50, 4.36		
C37	8.90	8.71	4.09	4.12	2.98, 3.20	
K38	9.38	9.29	4.61	4.61	1.85, 2.15	H^γ 1.39, 1.51; H^ϵ 3.21
C39	9.01	8.98	4.18	4.18	2.63, 3.18	
A40	8.91	8.77	4.30	4.30	1.57	
T41	7.25	*b*	4.73	4.73	4.75	$C^\gamma H_3$ 1.27
K42	9.41	9.23	4.11	4.19	1.85	H^γ 1.54; H^ϵ 3.02
E43	8.81	8.71	4.05	4.04	1.94, 2.15	H^γ 2.28, 2.42
E44	8.00	7.90	4.00	4.03	2.09, 2.22	H^γ 2.37
C45	8.53	8.46	5.22	5.21	2.92(*S*), 3.32(*R*)	
S46[d]	8.26	8.17	4.46	4.45	4.02, 4.05	
K47	7.12	7.11	4.44	4.46	1.92, 2.07	H^γ 1.55, 1.58
T48	7.99	7.97	4.23	4.18	*b*	$C^\gamma H_3$ 1.30
C49	8.85	8.79	4.66	4.67	2.78, 3.39	
T50	9.03	9.02	3.79	3.81	4.19	$C^\gamma H_3$ 1.31
K51	7.62	7.58	4.58	4.59	1.85	H^γ 1.54; H^δ 1.69; H^ϵ 3.01
P52		3.95		3.95	1.79, 2.26	H^γ 2.05, 2.10; H^δ 3.53, 3.79
C53	8.73	8.63	4.58	4.61	3.27(*R*), 4.09(*S*)	
S54	9.16	9.09	3.83	3.84	3.68	
C55	7.96	7.98	4.61	4.62	2.92, 3.11	
C56	7.29	7.23	4.81	4.81	3.02(*S*), 3.82(*R*)	
P57		4.41		4.41	1.66, 2.36	H^γ 1.43, 1.78; H^δ 3.36, 3.88
K58	8.52	8.30	4.10	4.13	1.68, 1.80	H^γ 1.37, 1.46

[a] For a few long-chain amino acids, all the side-chain proton resonances could not be located. [b] Could not be measured. [c] The cross peaks arising from the proton resonances of NH and H^α of N6, R26, and S46 overlap at 10 °C. [d] The cross peaks arising from the proton resonances of NH and H^α of Q12 and Q31 overlap at 30 °C.

Interproton Distance Restraints. NOEs were assigned from 2D NOESY spectra acquired with mixing times ranging from 60 to 150 ms. All of the assigned NOE cross peaks observed in the 60-ms NOESY spectrum were classified as strong, medium, or weak, corresponding to interproton distance restraints of 1.8−2.7, 1.8−3.2, and 1.8−3.6 Å, respectively (Williamson et al., 1985; Clore et al., 1986). Additional NOE cross peaks, which were observed in a spectrum acquired at a mixing time of 150 ms, were assigned distance limits of 1.8−4.5 Å. In all categories, the lower bounds for the interproton distance restraints were set to the sum of the van der Waals radii of two protons. Upper distance limits for distances involving methyl protons and nonstereospecifically assigned methylene protons were corrected appropriately for center averaging (Wüthrich, 1986), and an additional 0.5 Å was added to the upper distance limits for NOEs involving methyl protons (Clore et al., 1987; Wagner et al., 1987).

Torsion Angle Restraints and Stereospecific Assignments. Constraints on the backbone torsion angles, ϕ, were derived from the value of $^3J_{HN\alpha}$ measured in a high-resolution DQF-COSY spectrum. Torsion angle restraint ranges for ϕ were set to $-120° \pm 30°$ (for $^3J_{HN\alpha} > 9$ Hz), $-120° \pm 40°$ (for $^3J_{HN\alpha} = 9$ Hz), $-105° \pm 55°$ (for 8 Hz $\geq {}^3J_{HN\alpha} > 5$ Hz), and $-60° \pm 30°$ (for $^3J_{HN\alpha} \leq 5$ Hz). The preliminary analysis of the experimental NMR data suggests the absence of any α helix or β sheet in this protein. Therefore, the values of the $^3J_{HN\alpha}$ coupling constant between 5 and 8 were set to correspond to ϕ values in the $-105° \pm 55°$ range. This was set primarily to restrict the angle to the correct portion of the Ramachandran plot, except for those cases where there was a possibility of a type I β turn. For glycines, where the stereospecific assignment of the two Hα's was not made, and for prolines, where there is no amide proton, the backbone ϕ torsion angles were set to $-105.0° \pm 55.0°$ to allow for the maximum range. However, in cases where the preliminary analysis of the sequential and medium-range NOEs indicates the possibility of the presence of a type I β turn, the backbone ϕ torsion angles were open to cover the full possible range ($-40° \pm 140°$; ϕ varied from $-180°$ to 100°) (see supplementary material). This was done for Val10, Lys38, and Ala40. Stereospecific assignments for the β-methylene protons were made by analysis of the $^3J_{\alpha\beta}$ (measured in PE-COSY spectrum) and the intraresidue NH-β and $\alpha-\beta$ NOEs (Hyberts et al., 1987). In this way, stereospecific assignment of 12 out of a total of 18 cysteine $C^\beta H_2$ was made, providing 12 χ^1 torsion angle restraints.

Metal Cluster: A new "cluster" residue comprising of three Cd metal ions and nine cysteine Sγ atoms was defined in X-PLOR3.1. This residue contained the information about the coordinating sulfurs of each metal ion. The metal-to-protein connectivities were established from the analysis of $^1H-^{113}Cd$ HMQC data obtained on a ^{113}Cd-enriched metallothionein sample. Only the cysteine Sγ atoms were found to be involved in the coordination of the metal ions, and each metal ion was found to be ligated by four cysteine Sγs. Specific metal-to-cysteine connectivities (Narula et al., 1994) with assumed tetrahedral symmetry of each Cd ion were used as input for the structural calculations. A Cd−S bond length of 2.52 Å was used to represent the coordinate bond (Robbins et al., 1991).

Structure Calculations. All structure calculations were performed in the program X-PLOR3.1 (Brünger et al., 1986; Brünger, 1993; Kuszewski et al., 1992) on a SGI IRIS Indigo computer. Since this protein consisted of two separate structural domains (an N-terminal β domain and C-terminal α domain) with no NMR-observable interdomain interactions, the two domains were treated separately for structure calculations for computational time efficiency. The new "cluster" residue defined above in both the domains contained information about the metal−sulfur bonds and metal−sulfur−metal, sulfur−metal−sulfur, and cysteine C^β−sulfur−metal valence angles. The average value for these parameters was taken from the X-ray crystal structures of model cadmium(II) compounds and rat liver Cd_5Zn_2 MT-2 (Lacelle et al., 1984; Watson et al., 1985; Robbins et al., 1991). The values of the force constants used for the covalent geometry of the metal cluster were optimized by systematically varying these values to permit a dispersion in the geometrical parameters similar to that observed in the X-ray structure of rat liver Cd_5Zn_2 MT-2 (Robbins et al., 1991). The best values were found to be less than or equal to half of those defined for other heavy atoms in the program. The force constants selected in this way for sulfur−cadmium bonds and metal−sulfur−metal (and sulfur−metal−sulfur) valence angles were 500 kcal mol^{-1} Å^{-2} and 250 kcal mol^{-1} rad^{-2}, respectively.

The structures were calculated with the hybrid distance geometry/dynamical simulated annealing protocol (Nilges et al., 1988a). An initial set of 10 structures was generated by randomly selecting values for ϕ and ψ torsion angles. Each of these structures was used to produce a family of 10 embedded structures using the substructure distance geometry approach and all the experimental restraints. Each of these crude structures was taken through extensive regularization using template fitting and simulated annealing. Briefly, the procedure involved an initial Powell minimization of the random structures to remove any bad steric interactions, followed by extensive simulated annealing and a final round of Powell minimization. The target function that is being minimized during simulated annealing and conventional Powell minimization comprises only quadratic harmonic terms for covalent geometry (i.e., bonds, angles, planes, and chirality), square-well quadratic potentials for the experimental distance and torsion angle restraints (Clore et al., 1986), and a quadratic van der Waals repulsion term for the nonbonded contacts (Nilges et al., 1988a−c). Due to the limited number of experimental distance restraints, the force constant for NOE was selected to be 100 kcal mol^{-1} Å^{-2} instead of its normal recommended 50 kcal mol^{-1} Å^{-2}. All peptide bonds were constrained to be planar and trans. There were no hydrogen-bonding, electrostatic, or 6−12 Lennard-Jones empirical potential energy terms in the target function. A final round of annealing ensured that the structures were at equilibrium with respect to all potentials applied (vdW repulsion, bonds, angles, dihedrals, impropers, NOE and torsion angle restraints). The calculated structures were analyzed for the best fit to the NMR restraints and minimum value of overall energy. The selected best structures were further refined using simulated annealing refinement with a lower value of initial annealing temperature (500 K) and a reduced number of cooling steps (1000) (A. T. Brünger, private communication).

RESULTS

Resonance Assignments. Assignment of the proton resonances of blue crab MT-1 was performed by standard procedures as described in Wüthrich (1986). The first step involved the association of scalar-coupled resonances to specific spin systems using COSY, DQF-COSY, relay-COSY and TOCSY experiments, thus classifying the resonances according to their amino acid type. A long mixing time (τ = 155 ms) TOCSY on a MT-1 sample prepared in 99.8% ^2H_2O was particularly helpful for the assignment of the proton resonances from the long side chain amino acids. NOESY spectra were subsequently used to assign the spin systems to specific amino acids in the protein sequence. Even in the absence of any aromatic amino acid in the primary sequence, several spin systems could be identified that provided various starting points for the sequential connectivities. These included five threonines, four glycines, two alanines, and a unique valine at position 10. Figure 1 shows the fingerprint region of a COSY spectrum acquired at 10 °C. The assigned cross peaks are labeled by their one-letter amino acid code followed by their sequence number.

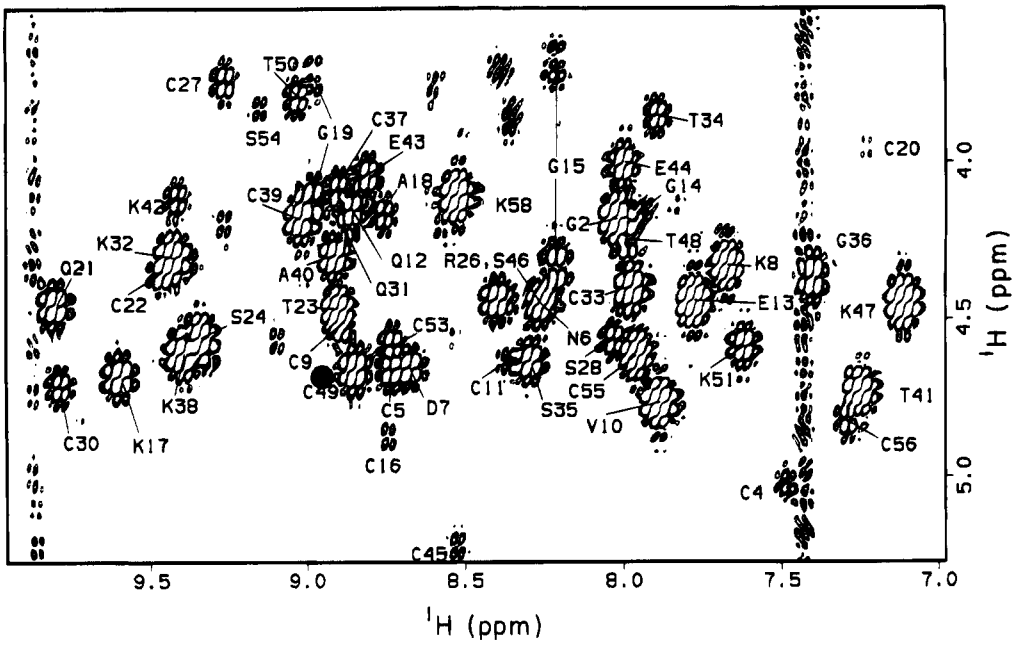

FIGURE 1: Fingerprint region of the phase-sensitive 2D ^{1}H−^{1}H COSY spectrum of a 4 mM sample of natural abundance cadmium substituted blue crab MT-1 at 10 °C in 90% H_2O and 10% ^2H_2O. The pH (uncorrected) of the sample is 7.0 in 20 mM KP_i. Both positive and negative levels are drawn without distinction. For this data set, 500 t_1 values, each with 72 scans, were acquired. The amino acid type and sequence number of each cross peak is indicated.

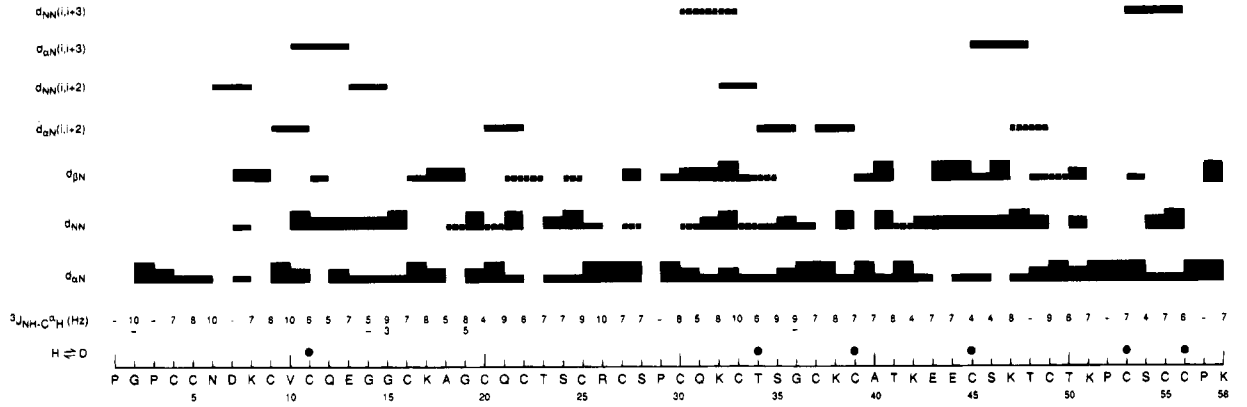

FIGURE 2: Amino acid sequence and a summary of sequential and medium-range NOE connectivities, $^3J_{NH\alpha}$ coupling constants, and slowly exchanging backbone amide protons (•) observed for blue crab MT-1. The solid lines are for a mixing time of 60 ms with the different widths reflecting the relative strength. Results from a longer mixing time (150 ms) data set are indicated by dashed lines.

Secondary Structure Analysis. A summary of all the sequential and medium-range NOEs observed in blue crab MT-1 is shown in Figure 2. Additional NOEs, which were observed in a NOESY spectrum acquired at the longer mixing time of 150 ms, are shown by dotted lines. A qualitative analysis of the medium-range NOEs indicates that while this protein lacks elements of regular secondary structure such as α-helix and β-sheet, there are six slowly exchanging backbone amide protons with combined NOE signatures that are indicative of β turns. The strong $d_{\alpha N}$ between C9 and V10 and the strong d_{NN} between V10 and C11 are suggestive of a type I β turn ending at C11. This is, however, not supported by the value of the $^3J_{HN\alpha}$ coupling constant for C9−V10. Similarly, the slow exchange of the backbone amide proton of C39, coupled with a strong $d_{\alpha N}$ between C37 and K38 and a strong d_{NN} between K38 and C39 is indicative of the presence of a type I β turn, which is again not supported by the $^3J_{HN\alpha}$ coupling constant between C37 and K38. Thus, while a preliminary qualitative analysis of the NMR data indicates the presence of β type turns, uncertainty arises as to whether the β turns are type I or II. The most characteristic difference between the two types of β turns is in the presence/absence of $d_{\alpha N}$ between residues 2 and 3 of the turn (present in type II β turn) resulting from a 180° flip in ϕ_3 (Wüthrich, 1986). This flip in ϕ_3 causes the amino proton of residue 3 of the turn to switch sides, and if there were long-range NOEs involving this amino proton, it might be possible to distinguish between these two turn possibilities when the full three-dimensional structure is calculated. Therefore, at the start of the structure calculations the allowed value of the angle ϕ for this residue in the turn was set to a very wide limit (−180° to 100°) to permit either structural element.

Structure Calculation. A summary of the long-range NOEs and the metal−to−cysteine connectivities obtained from the HMQC spectra on ^{113}Cd-substituted blue crab MT-1 is given in Figure 3. This figure clearly identifies the two separate metal binding domains in this protein and the absence of any interdomain interactions, which justifies the separate calculation of the structures of the individual protein domains. A set of 10 randomly generated structures was used to generate 100 embedded substructures for both the

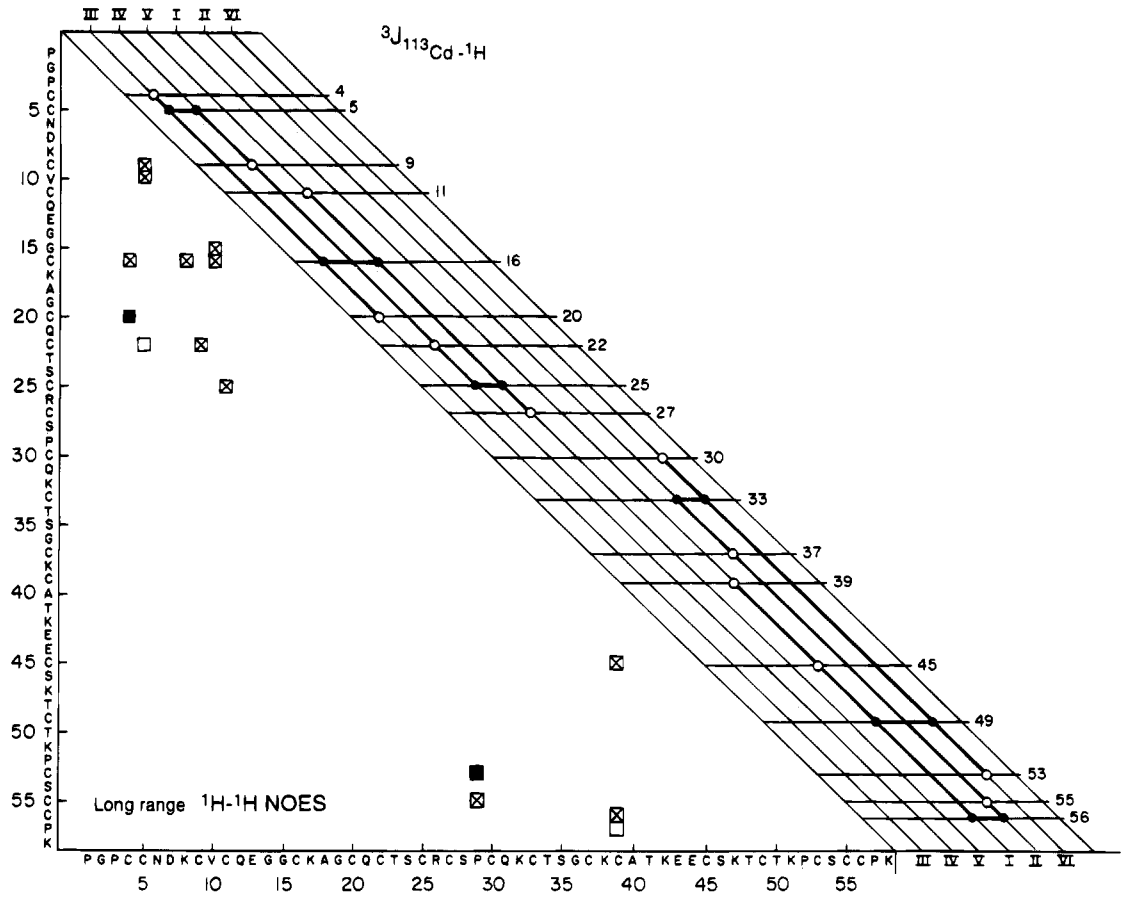

FIGURE 3: Combined plot showing long-range $^1H-^1H$ NOEs (lower left) and $^{113}Cd-S^{\gamma}$ J-coupling connectivities (upper right) used as input for the simulated annealing structure calculations of blue crab MT-1. The axes correspond to the protein sequence. A filled square at position (x,y) in the plane indicates at least one observed NOE between the backbone protons (NH or $C^{\alpha}H$) of the two residues in the sequence located at positions x and y. An open square indicates a NOE between the side-chain protons of the two residues, while a square with a cross in it indicates a NOE between the backbone amide proton or $C^{\alpha}H$ of one residue and the side-chain protons of the other residue. A filled circle indicates a bridging cysteine between two Cd(II) ions, and an open circle indicates a terminal cysteine and its liganding Cd(II) ion.

N-terminal and the C-terminal domain, each of which was regularized using template fitting and simulated annealing with the program X-PLOR as described under Materials and Methods.

The calculations for the N-terminal domain included the first 28 amino acid residues and the metal cluster formed by three cadmium ions and the Sγs of the nine participating cysteines. There were 115 experimentally derived inter-proton distances, 25 values of backbone torsion angles ϕ, and 7 values of side-chain torsion angle χ^1. The limits for the backbone torsion angle of Val10 were set in the range of $-180°$ to 100° as explained in Materials and Methods. After extensive regularization for the structures of the N-terminal domain, 56 structures had no distance violations greater than 0.5 Å and no backbone torsion angle violations of more than 5°. However, all of these structures did show 2−3 violations of the side-chain χ^1 torsion angle of cysteines, though these violations did not exceed 20° (Table 2). Many of these structures also showed violations of the covalent geometry parameters mostly in the metal cluster region, resulting in higher overall energy. For the final structural refinement, the 18 structures that showed the minimum overall energy were selected. These structures were further refined using a simulated annealing refinement with a lower value of the initial annealing temperature (500 K) and a reduced number of cooling steps (1000) (A. T. Brünger, private communication). The overall energy reduced only marginally after going through this step. The average structure was calculated from these 18 structures and its energy was again minimized with X-PLOR.

Table 2: Comparison of Input Side-Chain Dihedral Angles (χ^1) Obtained from NMR Data with Those Obtained from the Final 18 Simulated Annealed Structures

residue	input value and range (deg)	av value (deg) (rmsd)
C4	60.0 ± 30.0	38.6(2.8)
C5	*a*	−62.5(2.2)
C9	*a*	−165.9(1.9)
C11	180.0 ± 30.0	−142.4[b](0.4)
C16	−60.0 ± 30.0	−93.0[b](0.8)
C20	180.0 ± 30.0	−158.5(2.7)
C22	180.0 ± 30.0	152.7(2.5)
C25	60.0 ± 30.0	41.3(9.4)
C27	180.0 ± 30.0	−132.6[b](0.8)
C30	60.0 ± 30.0	50.0(1.9)
C33	−60.0 ± 30.0	−107.3[b](3.2)
C37	*a*	−171.2(1.5)
C39	*a*	−36.5(1.8)
C45	180.0 ± 30.0	−166.7(2.5)
C49	*a*	−30.3(16.0)
C53	−60.0 ± 30.0	−81.4(2.6)
C55	*a*	34.6(1.1)
C56	−60.0 ± 30.0	−34.9(2.1)

[a] The value of the side-chain dihedral angle (χ^1) could not be determined. [b] The value of χ^1 is violated.

Superposition of the backbone heavy atoms ($NC^{\alpha}C'O'$) for residues 4−27 along with the three Cd^{2+} ions and the C^{β} and S^{γ} of the coordinating Cys for the 18 final refined

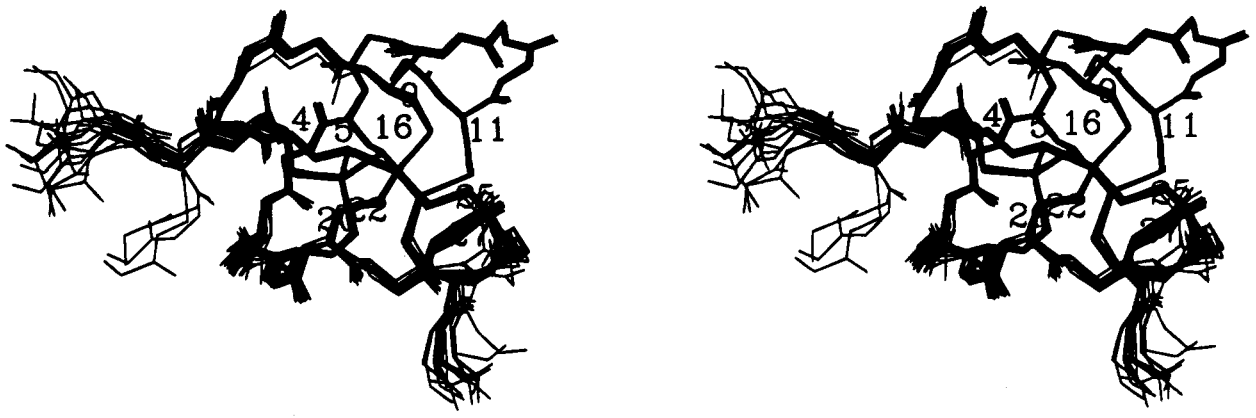

FIGURE 4: Stereoviews of the superpositions of the backbone heavy atoms ($NC^{\alpha}C'O'$) of the 18 final SA structures of the N-terminal domain of blue crab MT-1. The heavy atoms from residues 4−27 were considered for this superposition. The three cadmium metal ions (Cd3, Cd4, and Cd5) along with C^{β} and S^{γ} of the coordinating cysteines are also included in this illustration. The position of the C^{α} of each cysteine is numbered.

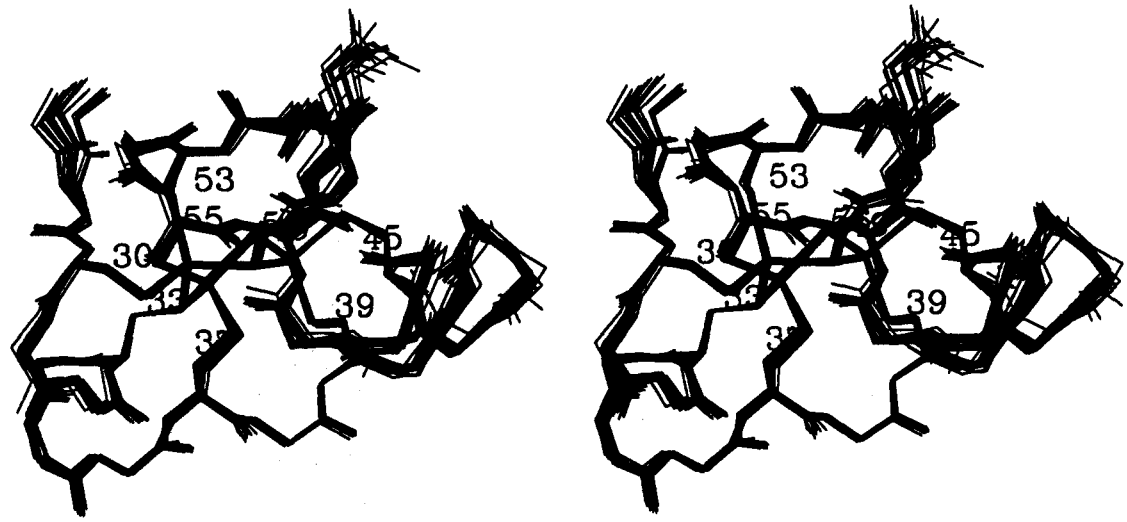

FIGURE 5: Stereoviews showing the superpositions of the backbone heavy atoms ($NC^{\alpha}C'O'$) of the 18 final SA structures of the C-terminal domain of blue crab MT-1. The heavy atoms from residues 30−56 were considered for this superposition. The three cadmium metal ions (Cd1, Cd2, and Cd6) along with C^{β} and S^{γ} of the coordinating cysteines are also included in this display. The sequence number of the C^{α} of all the cysteines is indicated.

structures is shown in Figure 4. Structural statistics are given in Table 3. With the exception of the N-terminal residues 1−3, other regions of the β domain are well-defined by the NMR data (Table 2 and supplementary material). The quality of the structures is reflected in the good overlap of the 18 structures and the small values of the rmsd (Table 3). The average pairwise rms difference for the backbone atoms ($NC^{\alpha}C'O'$) of residues 4−27 is 0.33 ± 0.13 Å.

The same protocol was used to obtain the structure of the C-terminal domain. The calculations for the C-terminal domain included 31 amino acid residues and the second metal cluster formed by three cadmium ions and nine S^{γ} of the participating cysteines. The last residue of the N-terminal domain, Ser28, was included in these calculations, as there was a short-range NOE observed from $C^{\alpha}H$ of S28 to the $C^{\gamma}H$ of P29. There were 163 experimentally derived interproton distances, 26 values of backbone torsion angles ϕ, and five values of side-chain torsion angle χ^1. The limits for the backbone torsion angle ϕ, of Lys38 and Ala40 were set in the range of −180° to 100° as explained in Materials and Methods. After extensive regularization for the structures of the C-terminal domain, 38 structures showed no NOE distance violations greater than 0.5 Å and no backbone torsion angle violations of more than 5° (supplementary material). However, there were violations of the side-chain torsion angle of the cysteine residues and covalent geometry parameters of the metal cluster atoms (Table 2). Among the acceptable structures, there are five structures which have values of ϕ in the positive range for Lys38 (93.2° ± 12.2°) and four structures which have values of ϕ in the positive range for Ala40 (103.0° ± 0.4°), indicating the possibility of a type II β turn. However, these structures had higher overall energy values (20% or more) and consequently were not selected with the final structures. The 18 best structures selected with the minimum overall energy all had these ϕ values in the negative region (supplementary material). These structures were refined further in the X-PLOR program. An average structure was calculated and was energy minimized using X-PLOR. Superposition of the backbone heavy atoms ($NC^{\alpha}C'O'$) for residues 30−56 along with the three Cd^{2+} ions and the C^{β} and S^{γ} of the coordinating Cys for the 18 final refined structures is shown in Figure 5.

Figure 6 plots a histogram of the rmsd for distance and torsion angle deviations versus sequence number for the final 18 refined structures, which enables the identification at a glance of the differences in the structure definition along the protein chain. The ϕ angle for Val10 in all the final 18 structures falls in the range of −106.0° ± 2.2°, even though

Table 3: Structural Statistics and Atomic rms Differences[a]

A. Structural Statistics

	⟨SA⟩	(SA)r
N-Terminal Domain (Residues 1−28)		
rms deviations from exptl distance restraints (Å)[b]		
all (115)	0.068 ± 0.002	0.066
interresidue sequential ($\|i-j\|=1$) (58)	0.069 ± 0.004	0.070
interresidue short range ($\|i-j\|\leq 5$) (5)	0.060 ± 0.007	0.057
interresidue long range ($\|i-j\|>5$) (20)	0.079 ± 0.004	0.074
intraresidue (32)	0.062 ± 0.002	0.057
rms deviations from exptl dihedral restraints (deg) (32)	3.333 ± 0.097	3.350
rms deviations from idealized covalent geometry used within X-PLOR		
bond (Å) (367)	0.009 ± 0.000	0.009
angles (deg) (675)	1.674 ± 0.016	1.650
impropers (deg) (174)	0.899 ± 0.917	0.900
selected X-PLOR energies (kcal/mol)[c]		
E_{bond}	23.04 ± 1.18	23.44
E_{angle}	176.80 ± 3.14	172.80
$E_{improper}$	21.42 ± 1.57	22.31
E_{NOE}	52.90 ± 2.73	50.51
E_{cdih}	23.46 ± 1.01	23.68
E_{repel}	18.00 ± 2.88	19.97
C-Terminal Domain (Residues 28−58)		
rms deviations from exptl distance restraints (Å)[b]		
all (163)	0.063 ± 0.001	0.058
interresidue sequential ($\|i-j\|=1$) (80)	0.056 ± 0.002	0.049
interresidue short range ($\|i-j\|\leq 5$) (34)	0.068 ± 0.004	0.063
interresidue long range ($\|i-j\|>5$) (10)	0.072 ± 0.004	0.073
intraresidue (39)	0.069 ± 0.002	0.067
rms deviations from exptl dihedral restraints (deg) (31)	0.163 ± 0.042	0.173
rms deviations from idealized covalent geometry used within X-PLOR		
bonds (Å) (445)	0.006 ± 0.000	0.007
angles (deg) (830)	1.373 ± 0.016	1.377
impropers (deg) (198)	0.854 ± 0.028	0.837
selected X-PLOR energies (kcal/mol)[c]		
E_{bond}	19.18 ± 0.71	18.34
E_{angle}	181.40 ± 2.33	178.95
$E_{improper}$	22.00 ± 1.44	21.14
E_{NOE}	65.07 ± 2.68	64.00
E_{cdih}	0.12 ± 0.06	0.12
E_{repel}	30.46 ± 1.92	30.52

B. Atomic rms Differences (Å)

	⟨SA⟩ vs $\overline{SA}$ N-terminal domain (residues 1−28)	⟨SA⟩ vs $\overline{SA}$ C-terminal domain (residues 28−58)
all atoms	2.09 ± 0.35	1.81 ± 0.20
backbone heavy atoms of all the residues	1.10 ± 0.45	0.39 ± 0.11
backbone heavy atoms of nonterminal residues	0.33[d] ± 0.13	0.34[e] ± 0.12
metal cluster atoms (3 Cd^{2+} and 9 S^{γ})	0.07 ± 0.05	0.06 ± 0.02

[a] The notation of the NMR structures is as follows: ⟨SA⟩ represents the final 18 simulated annealed structures; $\overline{SA}$ is the mean structure obtained by averaging the coordinates of the individual SA structures best fit to each other; (SA)r is the restrained minimized mean structure obtained by restrained regularization of the mean structure, $\overline{SA}$ (Nilges et al., 1988a). The number of terms for the various restraints is given in the parentheses. [b] None of the structures exhibited NOE-derived distance violations greater than 0.5 Å or backbone dihedral angle violations greater than 5°. [c] Energies were calculated by X-PLOR using a square well potential for the NOE term (100 kcal/mol Å^2) and a square well quadratic energy function for the torsional potential (200 kcal/mol rad^2). [d] All residues from C4 to C27. [e] All residues from C30 to C56.

the input range was very wide −40° ± 140° (supplementary material). This value of ϕ indicates that the β turn ending at C11 is of type I (supplementary material).

DISCUSSION

Quality of Structural Calculations. It has been shown from both NMR and X-ray studies of mammalian metallothioneins that these proteins lack any regular secondary structural elements (Arseniev et al., 1988; Schultze et al., 1988; Messerle et al., 1990; Robbins et al., 1991). The absence of these elements significantly reduces the interproton distance restraints present in NOESY spectra. In the published data on rat liver MT-2, a protein of 61 amino acids, only 126 NOEs were observed (Schultze et al., 1988). In the present studies on blue crab MT-1, a polypeptide of 58 amino acids, there were a total of 277 NOE restraints, of which 207 were intraresidue. The backbone torsion angles (ϕ) were determined for 51 residues using the experimentally measured $^3J_{HN\alpha}$. Stereospecific assignments for the Cys $C^{\beta}H_2$ and the estimation of the side-chain torsion angle, χ^1, could be made for only 12 out of 18 cysteines. The most important tertiary structural information came from the HMQC data, which revealed specific metal-to-cysteine connectivities for all six cadmium ions, leading to 24 additional Cd−S^{γ} restraints.

All of the above data along with the covalent geometry were used to arrive at a set of structures. The 18 best structures for the N-terminal and C-terminal domains are shown in Figures 4 and 5, respectively. The quality of the structures can be judged from the excellent overlap observed

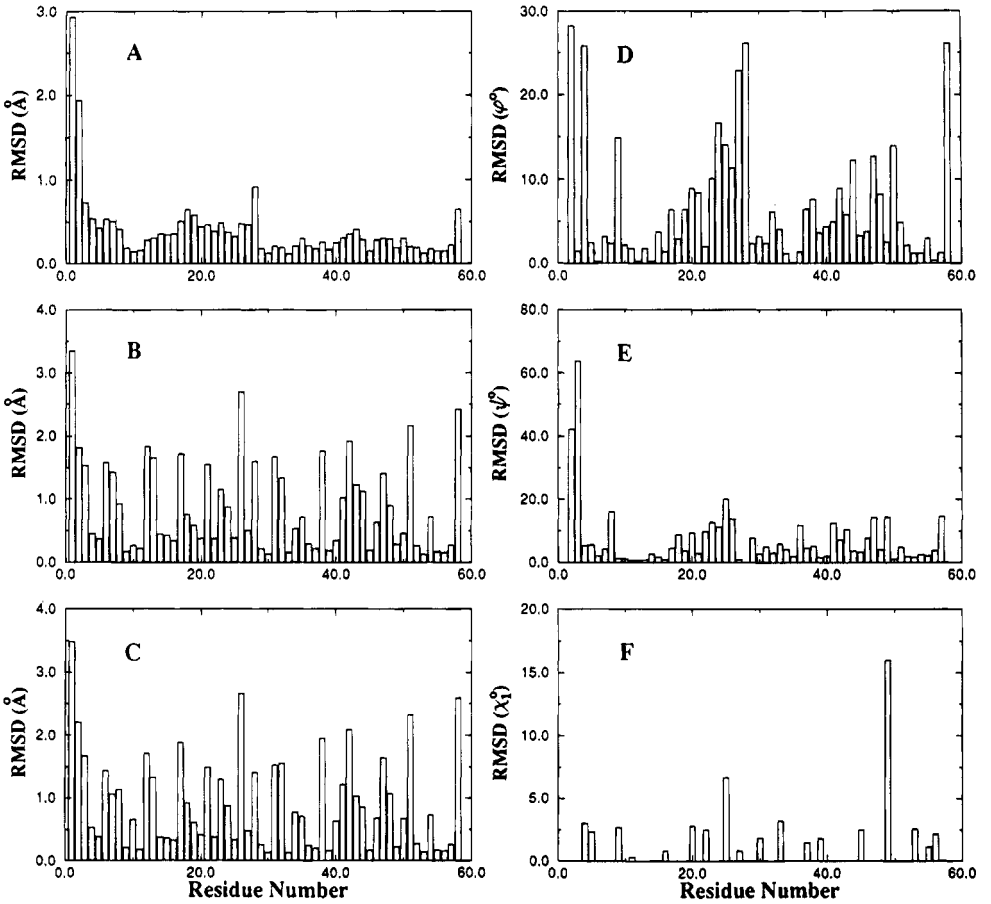

FIGURE 6: Histograms of rmsd values of the final 18 SA structures about the mean SA structure for the backbone heavy atoms (NC$^{\alpha}$C'O') (A), the side-chain atoms (B), and all atoms (C) as a function of residue number, and standard deviations of the backbone ϕ and ψ and the side-chain χ^1 torsion angles (D, E, and F, respectively) for the final 18 SA structures as a function of residue number.

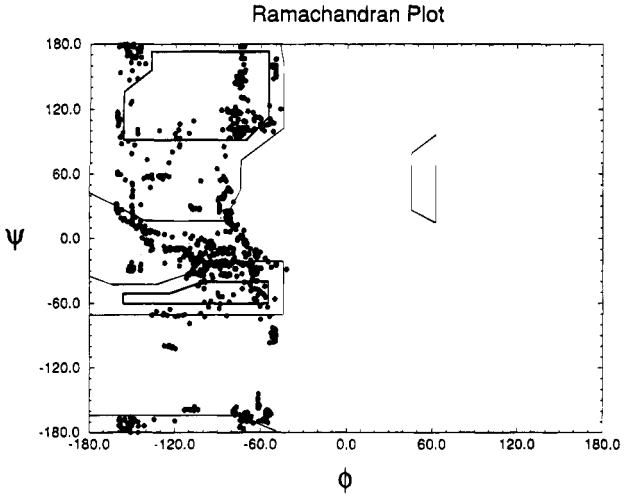

FIGURE 7: Ramachandran (ϕ, ψ) plot for the final 18 SA structures of both the N- and C-terminal domains of blue crab MT-1.

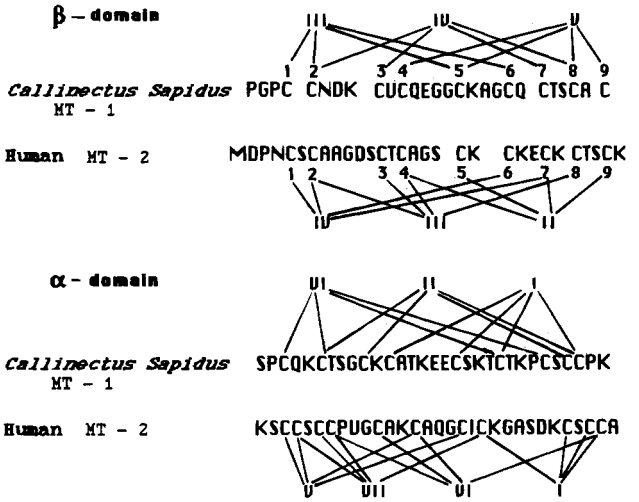

FIGURE 8: Primary amino acid sequence comparison of blue crab (*Callinectes sapidus*) MT-1 and human MT-2. Lines are drawn between specific metal ions and their coordinating cysteine thiols as established from $^1H-^{113}Cd$ heteronuclear multiple quantum coherence transfer experiments.

amongst all the structures of the set, which results in a small rmsd value for the backbone atoms of the various structures (Table 3). Additionally, all the backbone torsion angles are in the allowed space of a Ramachandran plot (Figure 7). The rmsd among backbone angles plotted in Figure 6 D, E shows a small variation for many residues of the protein with a somewhat larger variation occurring at the two termini and in the hinge region connecting the two domains of the polypeptide chain. Of the side-chain dihedral angles χ^1 determined for 12 out of a total of 18 Cys residues (Table 2), only four were violated consistently in all the final structures. Three of these violations were from Cys in the β domain, and one was from Cys in the α domain, and the magnitude of the violations varied from ~2° to 20°. For the six Cys residues for which the side-chain dihedral angle, χ^1, could not be experimentally measured, the final structures all showed a small value for their rmsd with the exception of Cys 49.

The rmsd for the backbone heavy atoms of each residue among the final structures indicates that the backbone is very

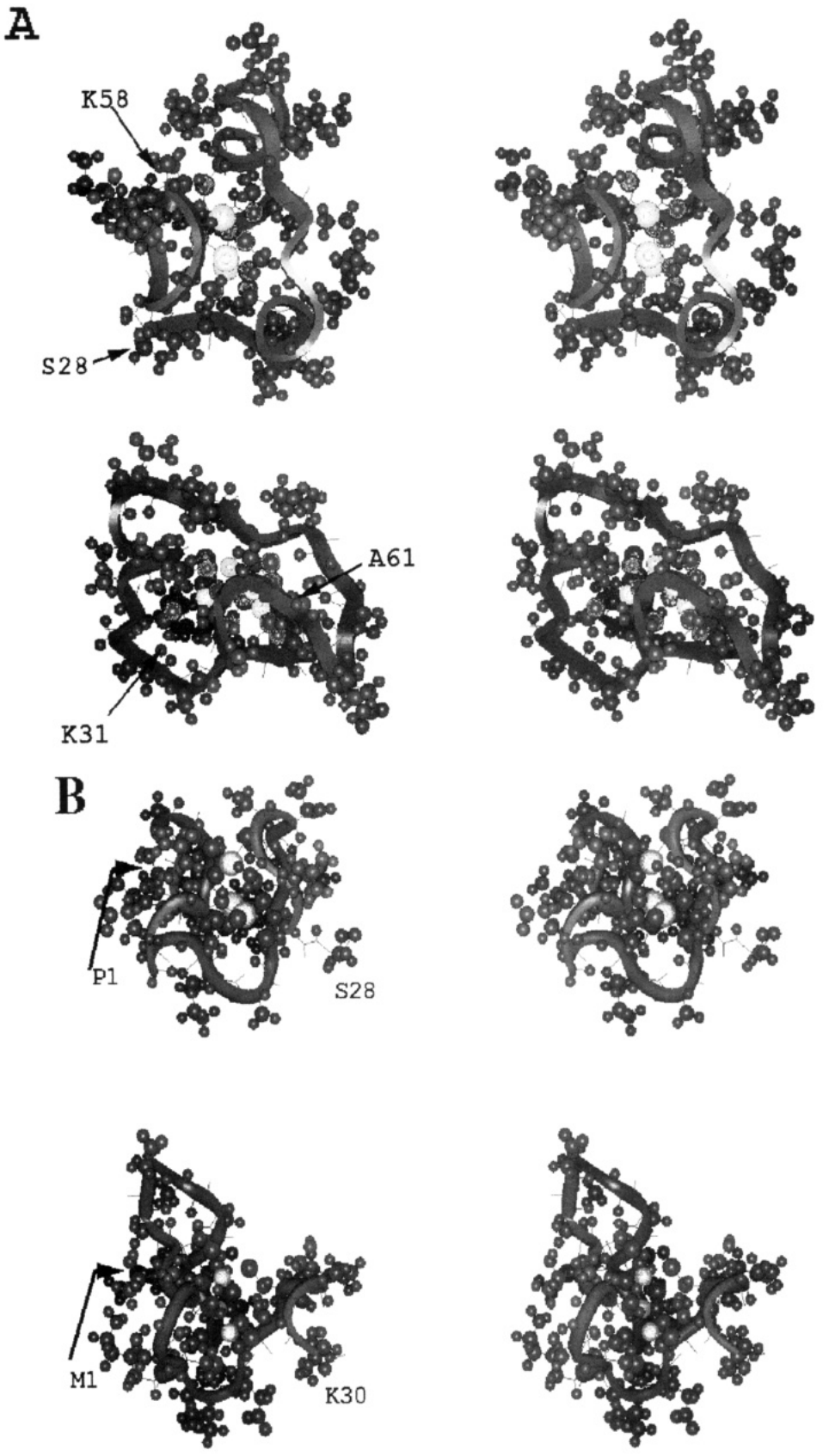

FIGURE 9: Stereoviews of the α (A) and β (B) domains of crab MT-1 (top) and human MT-2 (bottom). The ribbon outlines the backbone atoms, and the CPK models (scale = 0.4) denote the side chains and the metal ions (white). The N-termini are located on the left.

well constrained and defined, excluding the termini and the hinge region (Figure 6A). The situation worsens, however, when all the atoms of each residue or the side-chain heavy atoms of each residue alone are considered (Figure 6B,C; Table 3). This is especially true for amino acid residues with long side chains, e.g., Pro, Lys, Arg, Glu, and Gln, where relatively few distance restraints were obtained from the NMR data. It is reassuring, however, that the structures do not deviate significantly from their idealized covalent geometry, indicating that satisfaction of the pseudoenergy potentials for the NMR restraints has not led to unrealistic geometries (Table 3).

The analysis of the structural data indicates that the preferred value of ϕ for Val10 falls in the range of $-106° \pm 2.2°$ even though this angle was left wide open during structural calculations, where it could have opted for ϕ values suitable for a type II β turn (supplementary material). This final value demonstrates the presence of a type I β turn at K8−C9, V10−C11. Similarly, the backbone dihedral angle ϕ for Lys38 and Ala40 was left wide open (−180° to 100°), and yet the final 18 accepted structures all had their respective ϕ values in a narrow angular range (supplementary material). The preferred ϕ value for Lys38 is −98.9°, and for Ala40 it is −89.6°. These values indicate that these residues are also in type I β turns. However, 25% of the acceptable structures did have their ϕ values in the positive range, although all of these had a higher value of the overall energy (20% or more). In this domain, five backbone amide protons, four of which are cysteines, showed slow hydrogen−deuterium exchange indicating their involvement in hydrogen bonds. For each slowly exchanging backbone amide proton, the possible acceptor atoms (O, N, S) were evaluated on the basis of the following distance criteria (Metzler et al., 1993): NH···X distance, 2.0 ± 0.4 Å; HN···X distance, 3.0 ± 0.4 Å (where X can be an O, N, or S atom). Using these distance criteria and the average restrained structure, the potential hydrogen acceptor for the amide proton of Cys45 could be the backbone O atom of Thr41 (the NH···O and HN···O distances are 2.14 and 3.05 Å, respectively). Similarly, the potential hydrogen acceptor for the amide proton of Cys49 could be the backbone O atom of Cys45 (the NH···O and HN···O distances are 2.05 and 2.87 Å, respectively). The hydrogen bond acceptor for the other slowly exchanging amide protons, however (Cys11, Thr34, Cys39, and Cys56), could not be established.

That this is the first reported solution structure determination on a metallothionein from a nonmammalian source makes a structural comparison of the different species' MTs of particular interest. The alignment of the respective amino acid sequences for the invertebrate and human MTs is shown in Figure 8. Although the sequences of species' MTs are significantly different, the binding scheme between metals and cysteines is highly conserved in the β domain, with only three differences (crab Cd(III)−Cys(5)/human Cd(IV)−Cys(7), crab Cd(IV)−Cys(7)/human Cd(III)−Cys(4), and crab Cd(V)−Cys(8)/human Cd(II)−Cys(7)). Despite these minor differences in metal−cysteine coordination, the tertiary structure of crab MT-1 β domain bears a close resemblance to the same domain in mammalian MT-2.

Figure 9 shows a stereoview of the structures of crab MT-1 and human MT-2. The coordinates for human MT-2 (entries 1mhu and 2mhu) were obtained from the Protein Data Bank (Bernstein et al., 1977; Abola et al., 1987) at Brookhaven National Laboratory. The handedness of the crab MT-1 β domain proceeding from the N- to the C-terminus is right-handed, as it is in the human MT-2 β domain. Looking down the plane containing the three metal ions in both the crab MT-1 and the human MT-2 β domain (Figure 9B) shows the peptide chains divided into two sections: residues 1−23 and 24−30 in human MT-2 and residues 1−17 and 18−27 in crab MT-1 for the left- and right-hand sides of the plane, respectively. The fewer residues on the right-hand side of the plane defined by the metal ions in human MT-2 compared to crab MT-1 leaves the metal cluster in the former much more exposed with a wide cleft entering from the top center and a narrower one from the bottom. Much narrower and shallower clefts are found in the crab MT-1 extending from 5 to 11 o'clock (Figure 9B) and from 4 to 10 o'clock when viewed from the right (Figure 9B).

In the α domain of crab MT-1, the handedness is hard to describe because approximately half of the peptide is in a right-handed configuration and the other half is in a left-handed configuration (Figure 9A). The crab MT-1 α domain is more compact primarily as a result of the presence of only three metal ions. In this domain, there is evidence for a short α helix segment at position Lys42−Thr48 (Figure 9A). No clefts are visible extending into the metal-binding cluster, and the only exposure of the metal-binding cluster occurs on a surface that will be covered by the β domain in the intact protein.

From the above qualitative comparison of the structural elements in both domains of crab MT-1, one would predict more facile exchange of metal ions in the crab β domain compared to the α domain. This would be similar to what has been observed in the two domains of mammalian MT. This prediction, which is based upon an analysis of the tertiary structure, is supported by the line widths of the assigned ^{113}Cd NMR resonances from the two clusters (Narula et al., 1994). A further prediction from an analysis of the respective ^{113}Cd NMR spectra and the tertiary structures from both proteins is that the metal ions in the β domain of mammalian MT are more labile that those in the β domain of crab MT.

These structural studies have revealed the presence of two separate domains in *Callinectes sapidus* MT-1. Each domain contains a cluster of three metal ions, tetrahedrally coordinated to the S^{γ} of the nine Cys residues present in each domain. In total, six Cys residues participate in bridging two metal ions and twelve participate as terminal ligands. No interactions ≤ 4 Å are observed between the two protein domains, and the only element of regular secondary structure observed is the presence of several type I β turns.

ACKNOWLEDGMENT

We thank Mr. K. Gardner for computer software assistance, Prof. E. Lolis for the use of the Insight software for graphics purposes, and Mrs. Yufang Zheng for assistance in preparing some of the figures.

SUPPLEMENTARY MATERIAL AVAILABLE

Table showing a comparison of the input backbone dihedral angles (ϕ) obtained from the NMR data with those obtained from the 18 simulated annealed structures (3 pages). Ordering information is given on any current masthead page.

REFERENCES

Abola, E. E., Bernstein, F. C., Bryant, S. H., Koetzle, T. F., & Weng, J. (1987) Protein Data Bank, in *Crystallographic Databases—Information Content, Software Systems, Scientific Applications* (Allen, F. H., Bergerhoff, G., & Sievers, R., Eds.) pp 107−132, Data Commission of the International Union of Crystallography, Bonn/Cambridge/Chester.

Andersen, R. D., Taplitz, S. J., Oberbauer, A. M., Calame, K. L., & Herschman, H. R. (1990) *Nucleic Acids Res. 20*, 6049−6055.

Arseniev, A., Schultze, P., Wörgötter, E., Braun, W., Wagner, G., Vasák, M., Kägi, J. H. R., & Wüthrich, K. (1988) *J. Mol. Biol. 201*, 637−657.

Aue, W. P., Barthholdi, E., & Ernst, R. R. (1976) *J. Chem. Phys. 64*, 2229−2246.
Bauman, J. W., Liu, J., Liu, Y. P., & Klaassen, C. D. (1991) *Toxicol. Appl. Pharmacol. 110*, 347−354.
Bax, A., & Freeman, R. (1981) *J. Magn. Reson. 44*, 542−561.
Bax, A., & Davis, D. G. (1985) *J. Magn. Reson. 65*, 355−360.
Bax, A., & Drobny, G. P. (1985) *J. Magn. Reson. 61*, 306−320.
Bernstein, C. F., Koetzle, F. T., Williams, J. B. G., Meyer, F. E., Jr., Brice, D. M., Rodgers, R.J., Kennard, O., Shimanouchi, T., & Tasumi, M. (1977) *J. Mol. Biol. 112*, 535−542.
Brouwer, M., & Brouwer-Hoexum, T. (1991) *Arch. Biochem. Biophys. 290*, 207−213.
Brouwer, M., Brouwer-Hoexum, T., & Engel, D. S. (1984) *Mar. Environ. Res. 14*, 71−88.
Brouwer, M., Whaling, P., & Engel, D. W. (1986) *Environ. Health Perspect. 65*, 93−100.
Brouwer, M., Schlenk, D., HuffmanRingwood, A., & Brouwer-Hoexum, T. (1992) *Arch. Biochem. Biophys. 294*, 461−468.
Brouwer, M., Hoexum-Brouwer, T. M., & Cashon, R. E. (1993) *Biochem. J. 294*, 219−225.
Brünger, A. T. (1993) *X-PLOR Version 3.1 Manual*, Yale University, New Haven, CT.
Brünger, A. T., Clore, G. M., Gronenborn, A. M., & Karplus, M. (1986) *Proc. Natl. Acad. Sci. U.S.A. 83*, 3801−3805.
Butler, G., & Thiele, D. J. (1991) *Mol. Cell. Biol. 11*, 476−485.
Buttle, D. J., Ritonja, A., Pearl, L. H., Turk, V., & Barrett, A. J. (1990) *FEBS Lett. 260*, 195−197.
Cismowski, M. J., & Huang, P. C. (1991) *Biochemistry 30*, 6626−6632.
Cismowski, M. J., Narula, S. S., Armitage, I. M., Cherniak, M. L., & Huang, P. C. (1991) *J. Biol. Chem. 36*, 24390−24397.
Clore, G. M., Nilges, M., Sukumaran, D. K., Brünger, A. T., Karplus, M., & Gronenborn, A. M. (1986) *EMBO J. 5*, 2729−2735.
Clore, G. M., Gronenborn, A. M., Nilges, M., & Ryan, C. A. (1987) *Biochemistry 26*, 8012−8013.
Coleman, J. E. (1992) *Annu. Rev. Biochem. 61*, 897−946.
Cousins, R. J. (1985) *Physiol. Rev. 65*, 230−309.
Eich, G., Bodenhausen, G., & Ernst, R. R. (1982) *J. Am. Chem. Soc. 104*, 3731−3732.
Engel, D. W., & Brouwer, M. (1989) *Adv. Comp. Environ. Physiol. 5*, 53−75.
Freedman, J. H., Ciriolo, M. R., & Peisach, J. (1989) *J. Biol. Chem. 264*, 5598−5605.
Halliwell, B., & Gutteridge, J. M. C. (1990) *Methods Enzymol. 186*, 1−85.
Hamer, D. H. (1986) *Annu. Rev. Biochem. 55*, 913−951.
Hyberts, S. G., Marki, W., & Wagner, G. (1987) *Eur. J. Biochem. 164*, 625−635.
Jeener, J., Meier, B. Z. H., Bachmann, P., & Ernst, R. R. (1979) *J. Chem. Phys. 71*, 4546−4553.
Kägi, J. H. R., & Kojima, Y. (1987) in *Proceedings of the 2nd International Meeting on Metallothioneins and Other Low Molecular Weight Metal-Binding Proteins* (Kägi, J. H. R., & Kojima, Y., Eds.) Vol. 52, pp 25−61, Birkhäuser Verlag, Basel.
Kumar, A., Ernst, R. R., & Wüthrich, K. (1980) *Biochem. Biophys. Res. Commun. 95*, 1−6.
Kuszewski, J., Nilges, M., & Brünger, A. T. (1992) *J. Biomol. NMR 2*, 33−56.
Lacelle, S., Steven, W. C., Kurtz, D. M., Jr., Richardson, J. W., Jr., & Jacobson, R. A. (1984) *Inorg. Chem. 23*, 930−935.
Lerch, K., Hammer, D., & Olafson, R. W. (1982) *J. Biol. Chem. 257*, 2420−2423.
Marion, D., & Wüthrich, K. (1983) *Biochem. Biophys. Res. Commun. 113*, 967−974.
Marion, D., & Bax, A. (1988) *J. Magn. Reson. 80*, 528−533.
Messerle, B. A., Schäffer, A., Vasák, M., Kägi, J. H. R., & Wüthrich, K. (1990) *J. Mol. Biol. 214*, 765−779.
Metzler, W. J., Valentine, K., Roebbler, M., Friedrichs, M. S., Marsh, D. G., & Mueller, L. (1992) *Biochemistry 31*, 5117−5127.
Mueller, L. (1987) *J. Magn. Reson. 72*, 191−196.
Narula, S. S., Mehra, R. K., Winge, D. R., & Armitage, I. M. (1991) *J. Am. Chem. Soc. 113*, 9354−9358.
Narula, S. S., Brouwer, M., Enghild, J. J., & Armitage, I. M. (1994) *Magn. Reson. Chem. 31*, 96−103.
Nilges, M., Clore, G. M., & Gronenborn, A. M. (1988a) *FEBS Lett. 229*, 317−324.
Nilges, M., Gronenborn, A. M., Brünger, A. T., & Clore, G. M. (1988b) *Protein Eng. 2*, 27−38.
Nilges, M., Gronenborn, A. M., & Clore, G. M. (1988c) *FEBS Lett. 239*, 129−136.
O'Halloran, T. V. (1993) *Science 261*, 715−725.
Otvos, J. D., & Armitage, I. M. (1980) *Proc. Natl. Acad. Sci. U.S.A. 77*, 7094−7098.
Otvos, J. D., Olafson, R. W., & Armitage, I. M. (1982) *J. Biol. Chem. 257*, 2427−2431.
Otvos, J. D., Chen, S., & Liu, X. (1989) In *Metal Ion Homeostasis, Molecular Biology and Chemistry* (Winge, D., and Hamer, D., Eds.), pp. 197−206, Alan R. Liss, New York.
Piantini, U., Sorensen, O. W., & Ernst, R. R. (1982) *J. Am. Chem. Soc. 104*, 6800−6801.
Rance, M., Sorensen, O. W., Bodenhausen, G., Wagner, G., Ernst, R. R., & Wüthrich, K. (1983) *Biochem. Biophys. Res. Commun. 69*, 979−987.
Richards, R. I., Heguy, A., & Karin, M. (1984) *Cell 37*, 263−272.
Robbins, A. H., McRee, D. E., Williamson, M., Collett, S. A., Xuong, N. H., Furey, W. F., Wang, B. C., & Stout, C. D. (1991) *J. Mol. Biol. 221*, 1269−1293.
Sadhu, C., & Gedamu, L. (1988) *J. Biol. Chem. 263*, 2679−2684.
Schultze, P., Wörgötter, E., Braun, W., Wagner, G., Vasák, M., Kägi, J. H. R., & Wüthrich, K. (1988) *J. Mol. Biol. 203*, 251−268.
Seguin, C. (1991) *Gene 97*, 295−300.
Thiele, D. (1992) *Nucleic Acids. Res. 20*, 1185−1191.
Vallee, B. L., & Ulmer, D. D. (1972) *Annu Rev. Biochem. 41*, 91−128.
Vasak, M. (1986) *Environ. Health Perspect. 65*, 193−197.
Wagner, G., Braun, W., Havel, T. F., Schaumann, T., Go, N., & Wüthrich, K. (1987) *J. Mol. Biol. 196*, 611−639.
Watson, A. D., Rao, C. P., Dorfman, J. R., & Holm, R. H. (1985) *Inorg. Chem. 24*, 2820−2826.
Williamson, M. P., Havel, T. F., & Wüthrich, K. (1985) *J. Mol. Biol. 182*, 295−315.
Wüthrich, K. (1986) *NMR of Proteins and Nucleic Acids*, John Wiley & Sons, New York.
Zuiderweg, E. R. P., Hallenga, K., & Olejniczak, E. T. (1986) *J. Magn. Reson. 70*, 336−343.

BI941568L